ELSEVIER

Multi-color tunneling quantum dot infrared photodetectors operating at room temperature

G. Ariyawansa [a], A.G.U. Perera [a,*], X.H. Su [b], S. Chakrabarti [b], P. Bhattacharya [b]

[a] *Department of Physics and Astronomy, Georgia State University, Atlanta, GA 30303, United States*
[b] *Solid State Electronics Laboratory, Department of Electrical Engineering and Computer Science, University of Michigan,*
Ann Arbor, MI 48109-2122, United States

Available online 13 November 2006

Abstract

Quantum dot structures designed for multi-color infrared detection and high temperature (or room temperature) operation are demonstrated. A novel approach, tunneling quantum dot (T-QD), was successfully demonstrated with a detector that can be operated at room temperature due to the reduction of the dark current by blocking barriers incorporated into the structure. Photoexcited carriers are selectively collected from InGaAs quantum dots by resonant tunneling, while the dark current is blocked by AlGaAs/InGaAs tunneling barriers placed in the structure. A two-color tunneling-quantum dot infrared photodetector (T-QDIP) with photoresponse peaks at 6 μm and 17 μm operating at room temperature will be discussed. Furthermore, the idea can be used to develop terahertz T-QD detectors operating at high temperatures. Successful results obtained for a T-QDIP designed for THz operations are presented. Another approach, bi-layer quantum dot, uses two layers of InAs quantum dots (QDs) with different sizes separated by a thin GaAs layer. The detector response was observed at three distinct wavelengths in short-, mid-, and far-infrared regions (5.6, 8.0, and 23.0 μm). Based on theoretical calculations, photoluminescence and infrared spectral measurements, the 5.6 and 23.0 μm peaks are connected to the states in smaller QDs in the structure. The narrow peaks emphasize the uniform size distribution of QDs grown by molecular beam epitaxy. These detectors can be employed in numerous applications such as environmental monitoring, spectroscopy, medical diagnosis, battlefield-imaging, space astronomy applications, mine detection, and remote-sensing.

1. Introduction

In the field of infrared (IR) detector technology, quantum dot infrared photodetectors (QDIPs) have attracted the attention of researchers in developing devices with improved performances. Compared to quantum well infrared photodetectors (QWIPs), QDIPs have an extra degree of confinement, and hence they are expected to show lower dark current. Ranging from single element detectors [1–5] to focal plane arrays [6], QDIPs have already been demonstrated successfully. QDIPs are sensitive to normal-incidence infrared radiation, which is forbidden in n-type quantum well infrared photodetectors, based on the polarization selection rules. In addition, a long effective carrier lifetime in QDIPs, ∼100's of picoseconds, confirmed by theory [7] and experiments [8], provides the potential for highly sensitive devices. However, due to the unavailability of room temperature IR detectors, the commercial value of IR imaging systems have not been optimized yet. Even for QDIPs, the electron occupation is dominated by the excited states at temperatures above 150 K [9]. Therefore, in the conventional QDIPs, the reduction of the dark current is not significant at temperatures above 150 K. In general,

* Corresponding author. Tel.: +1 404 651 2847; fax: +1 404 651 1427.
E-mail address: uperera@gsu.edu (A.G.U. Perera).

any device structure designed to reduce the dark current, reduces the photocurrent as well. A novel design, the tunneling quantum dot infrared photodetector (T-QDIP)[10] uses resonant tunneling to selectively collect the photocurrent generated within the quantum dots, while the same tunneling barriers block the carriers contributing to the dark current. It is well known that the limiting operating temperature of the detector is connected to the dark current, which in turn relates to the detector response wavelength region. Ideally, the resonant tunneling approach can be used to develop IR detectors operating at high temperatures irrespective of the response wavelength region. Here, a room temperature T-QDIP, showing two color response at wavelengths of ∼6 and ∼17 μm is discussed.

Extending the idea, a terahertz (THz) T-QDIP detector operating at 150 K is also demonstrated. At present, the interest in the THz spectral region, 0.1–3.0 THz, has increased mainly due to the possible applications in the field of security. The development of THz sources elevates the demand for THz detectors. Due to the low energy associated with THz detection (<40 meV), any topical detector [11,12] having a reasonable detectivity will be working only at low temperature, since thermal excitations leading to high dark current take place at high temperature. This could be overcome by tunneling QDIPs, especially for THz detectors. THz radiation is absorbed in the active region of the structure and the excitations of carriers from a state in the dot to the resonant state in the quantum well would lead to the generation of photocarriers. In the THz region, the inhomogeneous size fluctuation of carriers would result in a wide spectral response in the wavelength space. Here, the successful results obtained on a T-QDIP THz detector operating at 6 THz (50 μm) at 150 K is reported.

A characteristic feature of any QDIP, where the QDs are well controlled over the size, is that they result in a narrow spectral response peaks. Also depending on the design, there can be more than one bound state in the system. As a result, QDIPs can yield several response peaks, which can then be called a "multi-color" detector. Besides different wavelength regions are associated with different practical applications, detecting an object's infrared emission at multiple wavelengths can be used to reduce the number of false positives. In this article, a detector design along with experimental results, in which there are two sizes of quantum dots (bi-layer QDs), is also presented. Each quantum dot yields one or two response peaks, and the detector can be used as a multi-color IR detector.

2. Experiment

The structures were grown by molecular beam epitaxy (MBE). The GaAs and AlGaAs layers were grown at 610 °C and the InGaAs or InAlAs quantum dot layers were grown at 500 °C. Vertical circular mesas for top illumination were fabricated by standard photolithography, wet chemical etching and contact metallization techniques.

The n-type top ring contact and the bottom contact were formed by evaporated Ni/Ge/Au/Ti/Au with thickness of 250/325/650/200/2000 Å. The radius of the optically active area is 300 μm. Devices for testing are mounted on to chip carriers with silver epoxy and gold wire contacts were made from the device to the chip carrier leads. Current–voltage (I–V) measurements were performed, by using a Keithley 2400 source meter, on all the mesas of the sample in order to check for uniformity of the structure. Spectral measurements for normal incidence radiation were carried out by using a Perkin Elmer System 2000 Fourier Transform Infrared (FTIR) spectrometer. The spectra were calibrated relative to a background spectrum obtained by a Si composite bolometer with the same set of optical components. The specific detectivity (D^*) of the devices at different temperatures and applied biases is obtained from the measured peak responsivity R_p and noise current density, S_i, measured with a fast Fourier transform (FFT) signal analyzer and a low noise pre-amplifier. A thick copper plate is used as the radiation block to provide the dark conditions for the measurements. Then D^* is calculated from $D^* = R_p A^{1/2}/S_i$.

3. Results and discussion

3.1. Tunneling-quantum dot infrared photodetector (T-QDIP)

The T-QDIP structure design for room temperature operation is schematically shown in Fig. 1. Self organized $In_{0.4}Ga_{0.6}As$ QDs were grown on a GaAs layer. $Al_{0.3}Ga_{0.7}As/In_{0.1}Ga_{0.9}As/Al_{0.3}Ga_{0.7}As$ serves as a double barrier. The band diagram under an applied reverse bias in shown in Fig. 2. The double-barrier resonant tunneling heterostructure serves to decouple the dark- and photocurrents. A single $Al_{0.1}Ga_{0.9}As$ barrier has been introduced on the other side of the dot to create a quantum well, in which well-defined quasi-bound final states are available for photoexcited electrons. The structure is designed so that these states resonate with the tunneling state in the

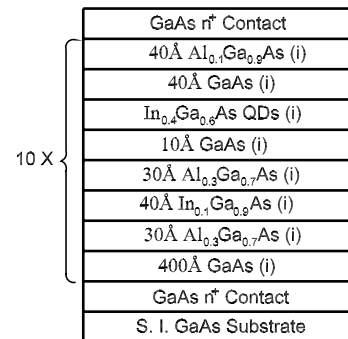| GaAs n⁺ Contact |
| 40Å Al₀.₁Ga₀.₉As (i) |
| 40Å GaAs (i) |
| In₀.₄Ga₀.₆As QDs (i) |
| 10Å GaAs (i) |
| 30Å Al₀.₃Ga₀.₇As (i) |
| 40Å In₀.₁Ga₀.₉As (i) |
| 30Å Al₀.₃Ga₀.₇As (i) |
| 400Å GaAs (i) |
| GaAs n⁺ Contact |
| S. I. GaAs Substrate |

Fig. 1. Schematic heterostructure of a T-QDIP grown by molecular beam epitaxy. InGaAs QDs are placed in a GaAs well. The AlGaAs/InGaAs/AlGaAs layers serve as a double-barrier to decouple the dark- and photocurrents. The letter i indicates that the layer is intrinsic.
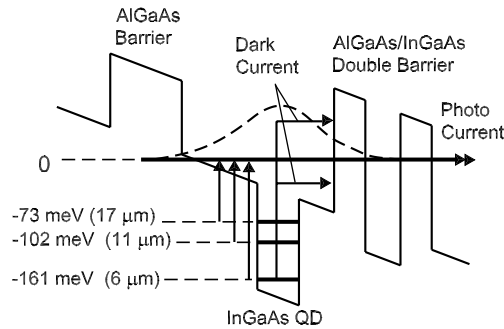
Fig. 2. Schematic diagram of the conduction band profile of the T-QDIP under reverse applied bias along with the calculated bound state energies in the dots and wells. The dark current channels are blocked by the barrier unless they happen to be excited to match the resonance level.

$Al_{0.3}Ga_{0.7}As/In_{0.1}Ga_{0.9}As/Al_{0.3}Ga_{0.7}As$ double barrier system. For photoexcited carriers with energy equal to the energy difference between QD bound state and well final state, the tunneling probability is near unity as confirmed by calculations. All other carriers excited to other states (contributing to the dark current) are blocked by the double barrier. In this way, a higher barrier for thermal excitations can be introduced, while the photoexcitation energy is very low. As a result, the operating temperature of the detector can be significantly increased. The energy states in the quantum dot, and the well were calculated by an eight-band $k \cdot p$ model [10], and solving the one dimensional Schrödinger equation including the presence of the wetting layer, respectively. Tunneling probability is calculated by the transfer matrix method.

The dark I–V characteristic of the T-QDIP structure at different temperatures (240–300 K), is shown in Fig. 3. The dark current densities at a bias of 1 V are 0.21, 0.96, and 1.55 A/cm^2 at 240, 280 and 300 K, respectively, and these values are lower than the dark current of other infrared detectors operating in comparable wavelength regions at the same temperatures. The spectral response measured with an applied bias of −2 V in the temperature range 240–300 K is shown in Fig. 4, and the responsivity at
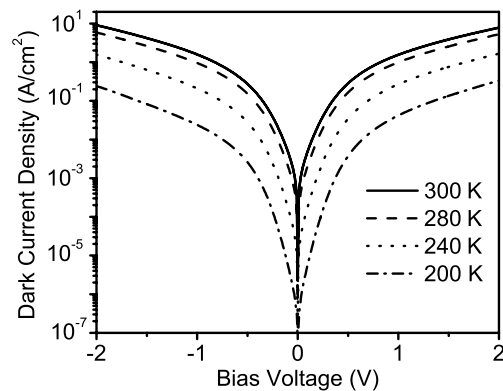
80 K under −4.5 V bias is shown in the inset. Two distinct peaks centered around ∼6 and ∼17 μm can be observed at high temperatures, and a weak response around 11 μm is also visible. The peak responsivity and the quantum efficiency of the 6 μm peak at 80 K and −4.5 V are ∼0.75 A/W, and 16%, respectively. As evident from Fig. 2, the peak at ∼6 μm is due to transitions from the ground state of the dot to the quasi-bound state in the well ($\Delta E = 161$ meV), whereas the 17 μm peak results from transitions from the second excited state of the dot to the quasi-bound state ($\Delta E = 73$ meV) in the well. The line-width, which corresponds to the inhomogenenous broadening of the QD states at 300 K, is ∼26 meV. Due to the symmetry of the dot geometry, the excited states in the QDs have a higher degeneracy (8) than the ground state (2). Therefore the number of carriers in the excited states compared to that in the ground state increases with the temperature although the occupation probability is lower. As a result, the 17 μm peak is dominant at high temperatures. The weak response at ∼11 μm corresponds to the energy separation between the first excited dot state and the well state ($\Delta E = 102$ meV). Furthermore, the specific detectivity, D^*, at 17 μm is on the order of 10^7 cm Hz$^{1/2}$/W at 300 K, and with some re-designing of the device heterostructure, a higher D^* can be achieved under the same conditions.

The same approach could be used to develop THz detectors operating at high temperatures. The schematic structure and the conduction band profile of the THz T-QDIP detector are shown in Figs. 5 and 6. In order to have a transition in the THz region within the structure, the bound state in the quantum dot should be close to the resonant state in the well. The possible way to achieve this is to form smaller QDs having two bound states. Then the QDs should be doped to raise the Fermi level so that photoexcitation can take place from the upper state in the dot to the resonant state in the well. In order to achieve this, $In_{0.1}Ga_{0.9}As$ QDs were grown mainly because the Al-containing islands (dots) are smaller in size compared to InAs

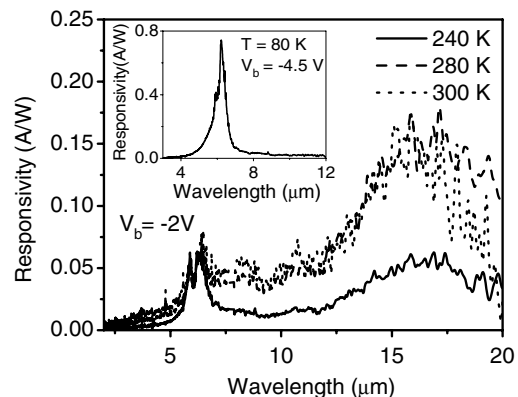Fig. 3. The dark current density as a function of bias in the temperature range 200–300 K.

Fig. 4. Spectral responsivity of T-QDIP in the temperature range 240–300 K under −2 V bias. Spectral responsivity at 80 K under a bias of −4.5 V is shown in the inset.
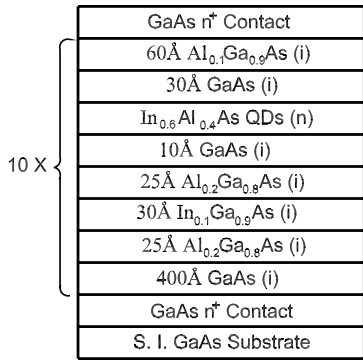
Fig. 5. Schematic heterostructure of a T-QDIP THz detector. $In_{0.1}Ga_{0.9}As$ QDs are n-doped with Si. $In_{0.1}Ga_{0.9}As$ was used in order to grow smaller QDs compared to InAs.
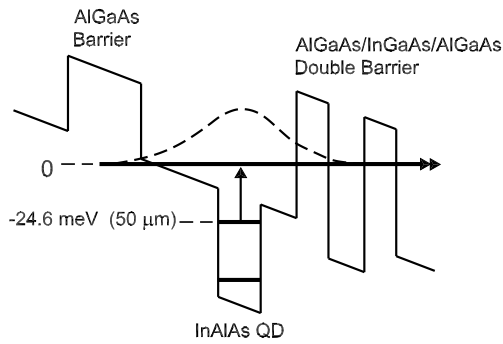

Fig. 6. Schematic diagram of the conduction band profile of the THz T-QDIP under reverse applied bias along with the calculated bound state energies in the dots and wells. The dark current channels are blocked by the barrier unless they happen to be excited to match the resonance level. Photoexcitation occurs from the second bound state in the dot to the resonant state in the well.

dots due to the smaller migration rate of Al adatoms on the growing surface during epitaxy.

The dark current density of THz T-QDIP at different temperatures is shown in Fig. 7. In the range shown, the T-QDIP detector shows a lower dark current density compared to other THz detectors operating in similar wave-
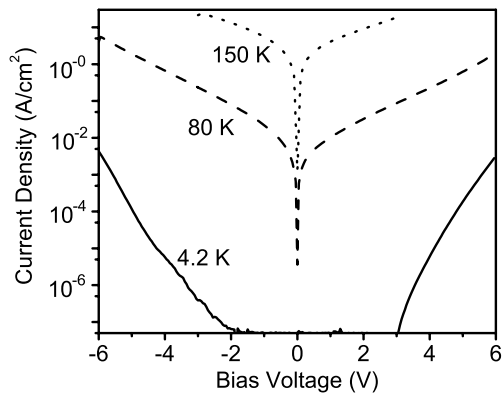

Fig. 7. The dark current density of THz T-QDIP as a function of bias in the temperature range 4.2–150 K.
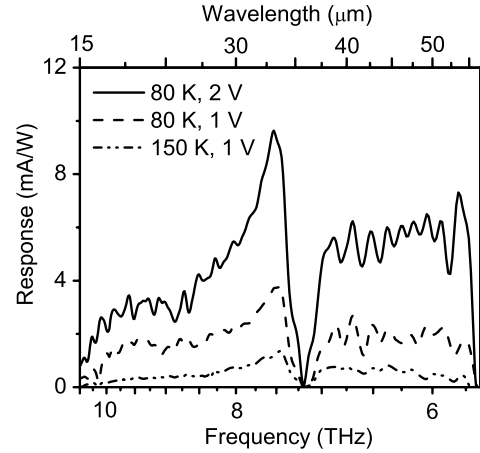

Fig. 8. Spectral responsivity of THz T-QDIP in the temperature range 80–150 K. The dip at 37 μm is the reststrahlen region of GaAs.

length regions. The spectral response of the detector at 80 and 150 K is shown in Fig. 8. The calculated energy difference between the two energy levels leading to the response is 24.6 meV (50.4 μm). Responsivity values at 80 and 150 K are 6 and 0.6 mA/W, respectively. The sharp dip around 37 μm is due to the reststrahlen band of GaAs, which reflects from every other GaAs based photon detectors [11,12]. The observed full-width at half maximum (FWHM) of the spectral response is 23 meV (3 μm), and this broadening arises due to the inhomogeneous size distribution of self-organized dots. Based on the results obtained, it can be concluded that the THz operation at high temperature (150 K) is made possible by the incorporation of resonant tunneling phenomena into the device design.
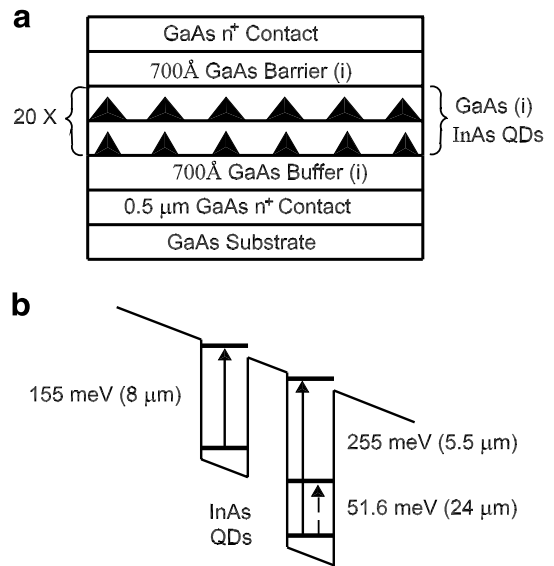

Fig. 9. (a) Schematic heterostructure of a bi-layer multi-color QDIP. On top of the first QD layer, another QD layer is grown, and the sizes of QDs in two layers are different. (b) Schematic diagram of the conduction band profile of the bi-layer QDIP. This also shows the energy states of two QDs with different sizes.

3.2. Bi-layer quantum dot infrared photodetectors

For multi-color detector applications, a QDIP which consists of two sizes of quantum dots, known as bi-layer QDIP, is presented. The detector structure with 20 periods of bi-layer QDs, and the conduction band profile of the structure are shown in Fig. 9. On top of the first (small) QD layer, another QD layer is grown so that the origin of the QDs in two layers are aligned. The size of the QD can be well controlled by the growth conditions. The larger QD consists of two bound states, while the smaller QD has three bound states. The energy states corresponding to each expected transitions are also shown in the figure.

The experimental spectral response of the detector in the mid infrared region (MIR) is shown in Fig. 10. There are two distinct peaks at 5.5 and 8 μm observed and these can be assigned to the transitions of electrons from the ground state to the top most state of the small and large QDs, respectively. The intensity of the second peak (8 μm) is weaker than that of the first peak, and this is probably due to inter dot tunneling of carriers since the ground state of the smaller dot is at a lower level compared

with the ground state of the larger dot. The response can be observed up to 140 K, as shown in the inset to Fig. 10. Moreover, a response in the far infrared (FIR) region is also observed, as shown in Fig. 11. This peak is probably due to the transition of carriers from the ground state to the first excited state of the smaller dot. Similar results for QDIPs in this wavelength region has been observed previously [13,14]. The intensity of the peak is strongly dependent on the applied electric field, and it is due to field assisted tunneling of strongly bound excited carriers. Similar to the MIR response, the FIR response can be observed up to 140 K. The major advantage of this design is attributed to the multi-color response of the detector.

4. Summary

In conclusion, T-QDIP detectors designed for toom temperature operation, and THz detection are reported. The high temperature operation is made possible by the incorporation of resonant barriers into the structure. A 17 μm detector that can be operated at room temperature, and a 6 THz detector operating at 150 K are successfully demonstrated. Moreover, a bi-layer QDIP consisting two quantum dot layers with two sizes of dots in the structure is also demonstrated. The detector shows multi-color response with peaks at 5.5, 8, and 24 μm. The response at all three wavelengths can be observed up to 140 K.
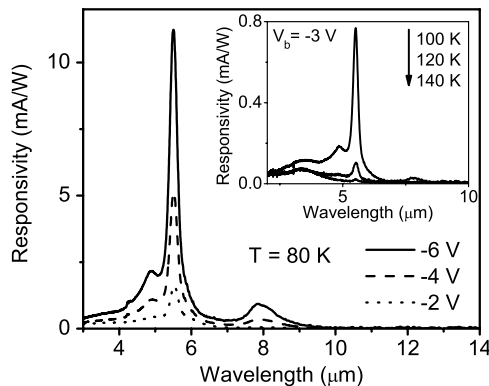
Fig. 10. Spectral responsivity of bi-layer QDIP in the MIR region at different temperatures, 80–140 K. Variation of the response with temperature is shown in the inset.
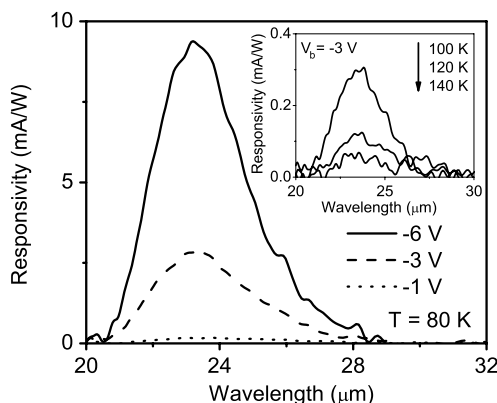

Fig. 11. FIR Spectral responsivity of bi-layer QDIP in the temperature range 80–140 K. Variation of the response with temperature is shown in the inset. This response is due to transitions of photoexcited carriers from the ground state to the first excited state in the smaller QD.

References

[1] B. Kochman, A.D. Stiff-Roberts, S. Chakrabarti, J.D. Phillips, S. Krishna, J. Singh, P. Bhattacharya, IEEE J. Quant. Electron. 39 (2003) 459–467.

[2] H.C. Liu, M. Gao, J. McCaffrey, Z.R. Wasilewski, S. Fafard, Appl. Phys. Lett. 78 (2001).

[3] L. Jiang, Sheng S. Li, Nien-Tze Yeh, Jen-Inn Chyi, C.E. Ross, K.S. Jones, Appl. Phys. Lett. 82 (2003) 1986–1988.

[4] S. Raghavan, P. Rotella, A. Stintz, B. Fuchs, S. Krishna, C. Morath, D.A. Cardimona, S.W. Kennerly, Appl. Phys. Lett. 1 (2002) 1369–1371.

[5] B. Aslan, H.C. Liu, M. Korkusinski, S.J. Cheng, P. Hawrylak, Appl. Phys. Lett. 82 (2003) 639.

[6] Sanjay Krishna, Darren Forman, Senthil Annamalai, Philip Dowd, Petros Varangis, Tom Tumolillo Jr., Allen Gray, John Zilko, Kathy Sun, Mingguo Liu, Joe Campbell, Daniel Carothers, Appl. Phys. Lett. 86 (2005) 193501.

[7] J. Urayama, T.B. Norris, J. Singh, P. Bhattacharya, Phys. Rev. Lett. 86 (2001) 4930.

[8] E. Kim, A. Madhukar, Z. Ye, J.C. Campbell, Appl. Phys. Lett. 84 (2004) 3277.

[9] P. Bhattacharya, X.H. Su, S. Chakrabarti, G. Ariyawansa, A.G.U. Perera, Appl. Phys. Lett. 86 (2005) 191106.

[10] H. Jiang, J. Singh, Phys. Rev. B 56 (1998) 4696.

[11] H. Luo, H.C. Liu, C.Y. Song, Z.R. Wasilewski, Appl. Phys. Lett. 86 (2005) 231103.

[12] M.B.M. Rinzan, A.G.U. Perera, S.G. Matsik, H.C. Liu, Z.R. Wasilewski, M. Buchanan, Appl. Phys. Lett. 86 (2005) 071112.

[13] S. Krishna, G. von Winckel, S. Raghavan, A. Stintz, G. Ariyawansa, S.G. Matsik, A.G.U. Perera, Appl. Phys. Lett. 83 (2003) 2745.

[14] S. Chakrabarti, X.H. Su, P. Bhattacharya, G. Ariyawansa, A.G.U. Perera, IEEE Photon. Technol. Lett. 17 (2005) 178.